MAPAN-JOURNAL ,
Publisher: METROLOGY SOC INDIA , NPL PREMISES,
Address: DR K S KRISHNAN MARG, NEW DELHI, INDIA,
ISSN / eISSN:0970-3950 / 0974-9853
Volume 25-Issue 1-(2025)
https://doi-001.org/1025/17666463849867

OPEN ACCESS

Article

Determination of the Shock Equation of State for Coral Sand and Analysis of Its Shock Wave Attenuation Characteristics

Kebin Li [1,2,*], Xuelei Shi [1] , Xiang Chen [3] and Xuhao Zhang[1]

Check for updates

[1] Key Laboratory of Impact and Safety Engineering, Ministry of Education of China, Ningbo University, Ningbo, Zhejiang, 315211, China
2 State Key Laboratory of Explosion Science and Technology, Beijing Institute of Technology, Beijing, 100081, China
3 State Key Laboratory of Precision Blasting, Jianghan University, Wuhan, Hubei, 430056, China

Fund:
This work was supported by the National Natural Science Foundation of China (Grant No. 12202217), Zhejiang Provincial Natural Science Foundation of China (Grant No. LMS25A020006), the Opening Project of State Key Laboratory of Explosion Science and Technology (Beijing Institute of Technology) (KFJJ21-19M) and the Natural Science Foundation of Ningbo,China (Grant No. 2021J122).

Abstract: In order to measure the Hugoniot data of coral sand easily and reliably, a new method for the Hugoniot data measurement is developed based on the impedance matching principle between the piezoconductive continuous resistance wire probe and the shock wave. In this paper, 8 groups of chemical detonation experiments with different impact strengths were carried out with emulsified explosives. The detonation wave and shock wave time history curves in explosives, PMMA, and coral sand were obtained through measurement and analysis. The results show that: for the study of high-pressure physics of large heterogeneous materials such as granular materials, the continuous pressure-conducted probe can bring great convenience to the field measurement of shock waves. The measured parameters were simulated by autodyn simulation software to simulate the attenuation effect of coral sand under a certain equivalent TNT explosion shock wave.

Keywords: Coral sand; Hugoniot; Continuous resistance probe; Chemical explosion

Citation: To be added by editorial staff during production.

Academic Editor: Firstname Lastname

Received: date
Revised: date
Accepted: date
Published: date

1. Introduction

Calcareous sand is the biological sediment and skeletal remains of Marine organisms, the main component of which is calcium carbonate. They are widely distributed in the South China Sea Islands, the Red Sea, the southern Arabian Gulf, the western waters of India, the western continental shelf of Australia, Bass Strait, the Java Sea, the waters of Florida in North America, the waters of Central America and Barbados. Coral sand is characterized by high porosity, loose fragmentation, easy consolidation of particles, and low hardness, which makes its engineering mechanical properties very different from common continental and Marine sediments [1-3]. These material properties bring many difficulties to the construction of coral reef projects.

Due to the special Marine biological origin of coral sand, the shape of coral sand particles is irregular and rich in internal pores. Particles can generally be divided into blocky, flakelike, clad-like, and irregular shapes [4]. There are more isolated closed pores in the particles, and the diameter of the pores has a power function relationship with the tightness and a linear relationship with the sphericity [5]. The analysis of the shape factors after particle breakage shows self-similarity and scale-free of particle breakage, which

leads to the evolution of particle gradation toward the fractal breakage limit with the increase of pressure [6]. The three-dimensional microscopic pore properties of porous media are determined by the microscopic morphology of the particles in the medium. Irregular particle shape leads to regular pore shape. The roughness of the particle surface results in small pore size. Small throat radius due to irregular particle shape; The roughness of particle surface leads to poor media connectivity. The regularity of particle shape results in uniform pore distribution [7].

In order to obtain the mechanical properties of calc sand, domestic and foreign scholars have conducted a large number of indoor geotechnical tests, such as the basic physical and mechanical properties test [8-9], uniaxial compression test [10-16], triaxial isotropic consolidation test [17-18], and dynamic triaxial test [19-21]. However, although many basic physical and mechanical properties of calcareous sand can be obtained through a large number of laboratory experiments and theoretical model studies, our understanding of calcareous sand is still in the preliminary stage.

In order to ensure the safety of Marine engineering construction, Marine protection engineering is becoming more and more important. In the face of unexpected explosive loads and strong impact, coral sand is the main bearer. Therefore, it is of great significance to study the impact compression characteristics of coral sand for the protection engineering of islands and reefs and Marine engineering. However, at present, scholars have done a lot of research on terrigenous sand sand, but have little understanding of the impact compression characteristics of coral sand. Gang Zhou et al. [22] made a sample with a diameter of 54mm and a thickness of 54mm. Through the plate impact test, an electromagnetic particle velocity sensor was used to obtain the impact adiabatic data of loess with different moisture content. M. Arlery et al. [23] made a sample with a diameter of 100mm and a thickness of 15mm. Through the plate impact test, VISAR and an electric probe were used to measure the impact Hugoniot state of partially water-saturated silica sand. J. W. LaJeunesse et al. [24] made a sample with a diameter of 60mm. The effects of grain size and water content on the dynamic macro response of 5mm thick silica sand were investigated by means of VISAR, PDV, PVDF, and velocity probes. Ding Yuqing et al. [25] studied the impact compression characteristics of unsaturated clay samples with different water contents by combining magnetic velocity measurement and fiber probe dynamic testing techniques for samples with a diameter of 16mm and a thickness of 3mm. Similarly, there is literature [26-29]. It can be seen that most scholars at home and abroad carry out flat plate impacts on small specimens and obtain shock wave parameters by optical or electrical methods. However, these methods have some shortcomings: (1) Due to the significant non-uniformity and high porosity of granular materials, the dynamic response characteristics are greatly affected by the particle size, so it is necessary to ensure that the sample has a large enough "macro" size, and the light gas gun loading limits the sample size. (2) The measurement means in the laboratory, although the accuracy is high, the operation is complex, the test cost is high, coupled with the limitations of equipment protection, lighting sources, etc., it is not economical and convenient. In this paper, a continuous resistance measurement method of coral sand impact equation of state is proposed, which can achieve large size, economical, and convenient measurement.

2. Experimental methods

2.1. Material

The coral sand used in the test comes from the South China Sea. It is a special granular rock and soil material, mainly composed of calcium carbonate. Its porosity is large. According to the "Geotechnical Test Procedures", the samples were selected for the screening test and specific gravity test, and the grading curve of coral sand particles could be obtained from the cumulative mass percentage, as shown in Fig. 1. The relevant physical

property parameters are shown in Table 1, in which D_{60} represents the particle size corresponding to 60% of the ordinate on the grading curve, D_{30} represents the particle size corresponding to 30% of the ordinate on the grading curve, D_{10} represents the particle size corresponding to 10% of the ordinate on the grading curve, C_u represents the uniformity coefficient, and C_c represents the curvature coefficient.

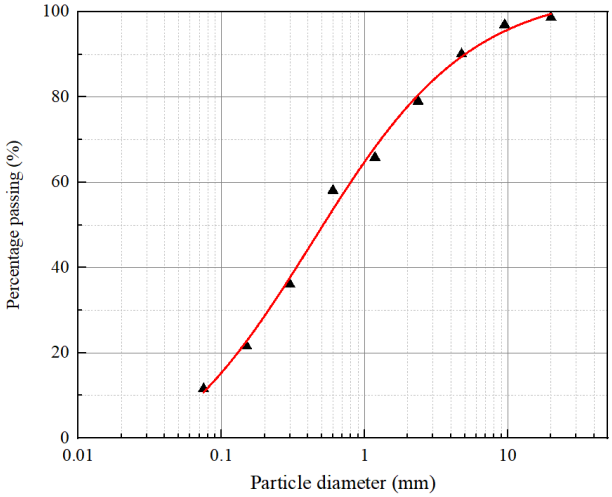

Fig. 1 Coral sand grading curve

Table 1. Coral sand sample parameters

D_{60}/mm	D_{30}/mm	D_{10}/mm	C_u	C_c
0.75	0.21	0.06	12.8	0.98

2.2. Quasi-static compression

2.2.1. sample preparation

Considering that the morphology and porosity of coral sand with different particle sizes are quite different, to further understand the compression performance of coral sand with different particle sizes,6 groups of coral sand with different initial particle sizes are selected as test materials (Fig. 2). Recorded as A1-A6, A1: <0.5mm, A2:0.5-1mm, A3:1-2mm, A4:2-3mm, A5:3-4mm, A6:4-5mm. The six groups of coral sand were all loaded and molded with 5mm thick steel sleeves.3 groups of coral sand with each particle size were set up for repeated tests, and the test results were averaged. In addition, the scanning electron microscopy (SEM) micrographs are shown in Fig. 3.

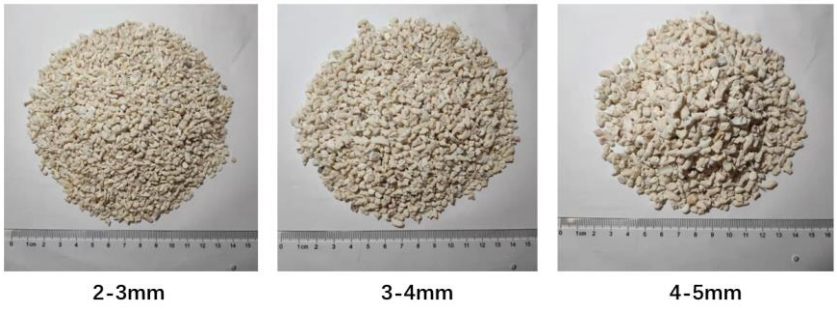

Fig. 2 Prepared coral sand sample

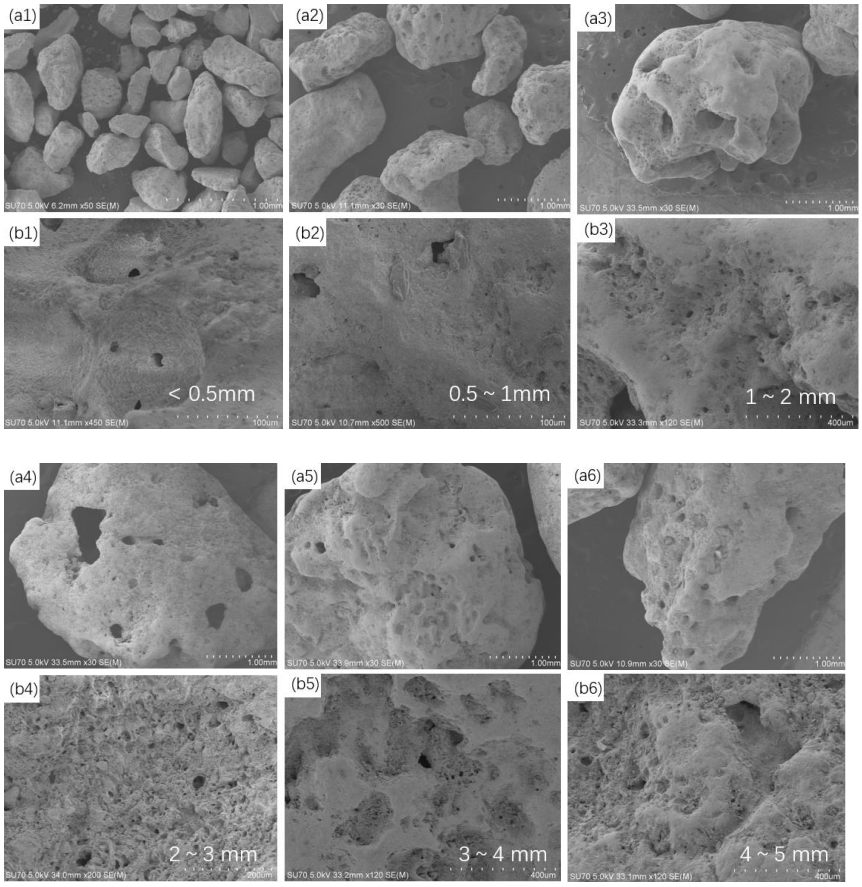

Fig. 3 SEM of prepared coral sand sample

2.2.2. Equipment

The quasi-static compression test adopts MTS Landmark (Fig. 4). The Inner diameter of the sleeve is 37.1 mm. The length of the pad is 62mm, the diameter of the pad is the same as that of the sleeve, and the thickness is 7mm. The base for fixing the sleeve and the indenter for pressure are also provided above and below the sleeve.

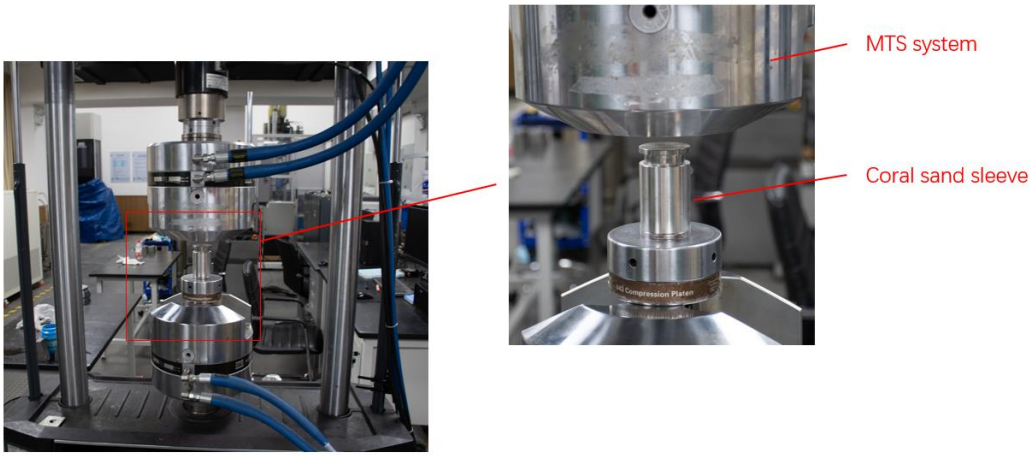

Fig. 4 Universal material testing machine MTS

2.2.3. Test results

Fig. 5 is the test principle diagram of the MTS and sleeve. The pre-pressed coral sand sample is moved to the MTS, and a uniform pressure of 0.02mm/s is applied. The upper-end face of the testing machine is in contact with the pressure head of the sleeve, and the data of pressure and displacement changes with time during loading are obtained through the control interface. After reaching the end pressure, the loading force of the testing machine is automatically unloaded, and the sleeve is removed to take out the compressed coral sand sample and recover it. In order to reduce the dispersion of the test, the three sets of tests were repeated for the coral sand samples with the same particle size group to obtain the average value, and finally, the stress-strain curves of each particle size could be obtained (Fig. 6). The sample was carried out at a termination pressure of 120kN. As can be seen from the figure, the variation trend of stress with strain is from slow to sharp. In the initial stage of compression, the pores between coral sand particles are large, and the stress value increases slowly with the increase of strain, which is mainly a process of compression of pores. When the pores in the sample are compressed relatively small, the contact force between particles increases. The stress of the coral sand sample starts to increase greatly, and in the second half of loading, the coral sand particles will be broken. When the coral sand particles are broken to a large extent and the pore compression between the particles is small, the stress of the sample increases more and more. Therefore, the overall curve shows that the stress increases slowly with the strain at the initial loading stage, and the stress increases significantly with the increase of strain when the strain increases to a certain value.

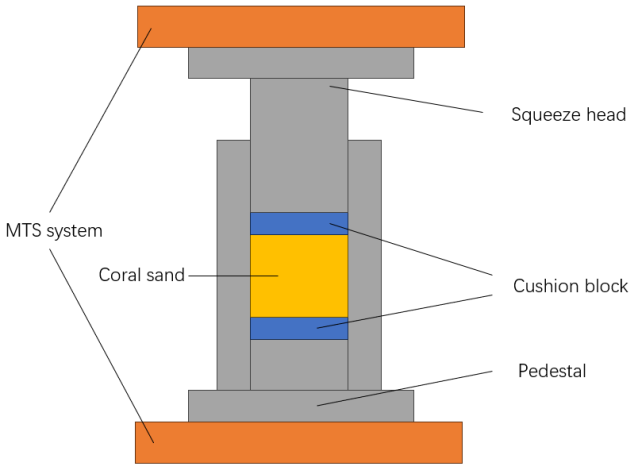

Fig. 5 Assembly diagram

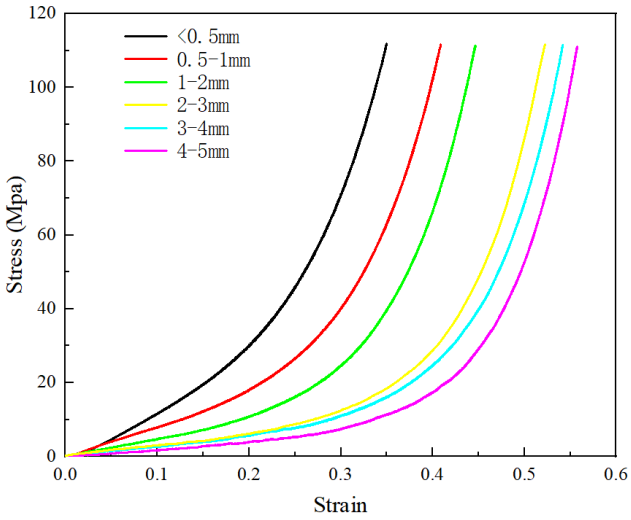

Fig. 6 Static compression curves of coral sand with different particle sizes

The static compressive stress-strain curve of coral sand contains five different deformation processes inside the material: elastic compression deformation of contact between particles, mutual sliding and rotation of particles when the material skeleton is crushed, re-interlocking of particles, obvious particle breakage beginning and particle breakage ending. As can be seen from Fig. 5, the front of the compression curve of particle size <0.5mm rises quickly, because the particle size is small, the coordination number of particles is high, the pores of small particles are small, and the particles are not easy to be destroyed as a whole. As a result, the first three stages occur quite quickly, and the stress of the particles rises immediately, making them enter the obvious crushing stage. It can be seen from the figure that the same strain, the stress of small particles is greater, that is, small particles need to absorb more energy when broken. The speed of particle rearrangement is related to particle size, the smaller the particle and the easier it is to translate and rotate, the smaller the particle size between the particles limits the movement distance of the particle, which is conducive to the rapid rearrangement of the particle and the formation of a stable force chain, which is reflected in the curve bend, the small particle will turn faster and have higher stress. When the particles are broken, the rearrangement of the particles makes more small particles share the pressure, and the bearing capacity of the granular particles is further improved. After the curve turns, the crushing rate of the particles is very low, and the particles are pressed very densely, so the material appears hardened. Since the grading of large particles is wider and better after crushing, it shows a greater stiffness in the macro view, so with the same stress level, The stiffness of large particle size is greater.

2.3. Dynamic experimental apparatus

2.3.1. Flexible continuous resistance probe

Shock wave measurement techniques generally include optical methods, electronic methods, pulse X-ray photography, and recovery methods, of which the most commonly used are optical methods (scanning mirror method and flash gap method, etc.) and electronic methods (resistance wire method and foil probe method, etc.). The continuous resistance test method used in this paper has been applied many times in the measurement of shock wave [31-33] and has a good application prospect. Compared with the discrete electric probe measurement, the probe has higher measurement accuracy. Compared with commercial continuous probes, the probe has higher test stability, reliability, and anti-interference ability [34].

The structure of the pressure conductance continuous resistance probe is shown in Fig. 7.

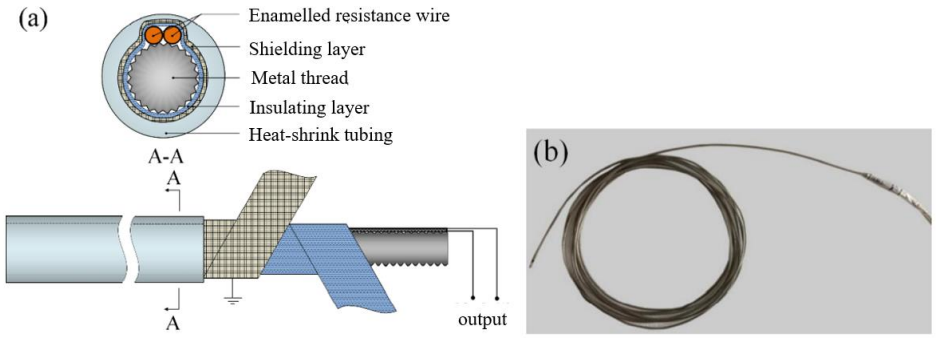

Fig. 7 Schematic illustration of continuous pressure- conducted probe

2.3.2 Shock wave measuring set

The whole device is divided into three parts, supported by a wooden frame. As shown in Fig. 8, one end is explosive with a diameter of 100mm and a length of 250mm, and the back end is coral sand sample with a layer of PMMA in the middle.

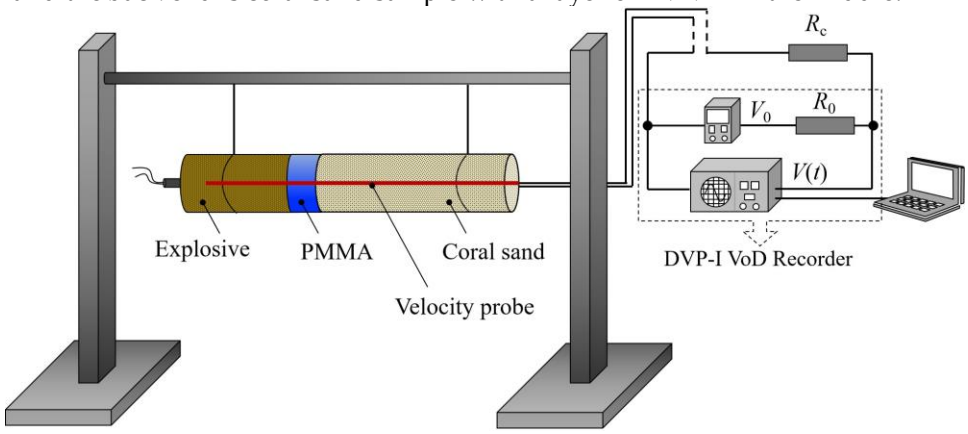

Fig. 8 Shockwave device diagram

The test system composed of the pressure conductance probe and the detonation velocity meter is also shown in Figure 8, where *R*c is the loop cable resistance, R_0 is the internal resistance of the instrument, and the resistance of the probe will change *R*(t) with time due to the process of the shock wave.

When given constant pressure V_0, there is

$$V(t) = \frac{R(t) + R_c}{R(t) + R_c + R_0} V_0 \tag{1}$$

If the resistance value per unit length of the resistance wire r_p is known, the length of the probe that is conductive by detonation wave pressure can be obtained according to formula (1)

$$L(t) = L_{p0} - \frac{R(t)}{r_p} = \frac{R_a + R_c + R_0}{r_p} - \frac{R_0 V_0}{r_p (V_0 - V(t))} \tag{2}$$

2.4. Determination of the shock equation of state

2.4.1. Experimental scheme

To measure the impact Hugoniot line of coral sand, eight sets of shock wave experiments will be carried out, and the shock wave intensity will be adjusted by changing the thickness of the PMMA. The shock wave information in each set of explosives, PMMA, and coral sand can be obtained by using the shock wave velocity measurement device (Fig. 9), and the time history curve of the shock wave in each medium can be obtained by analyzing the electrical signal. Then the shock wave state in each group of coral sand is obtained by the impedance matching principle, that is, the shock state of coral sand under an impact intensity is obtained. The Hugoniot line of coral sand impact can be fitted by processing the 8 data. The basic parameters of 8 experiments are shown in Table 2：

Table 2. Basic parameters of coral sand samples for 8 experiments

Number	Quality m_c (kg)	Density ρ_c ($g \cdot cm^{-3}$)
1	3.67	1.406
2	3.655	1.441
3	3.57	1.435
4	3.405	1.402
5	3.5	1.337
6	3.545	1.374
7	3.56	1.392
8	3.8	1.398

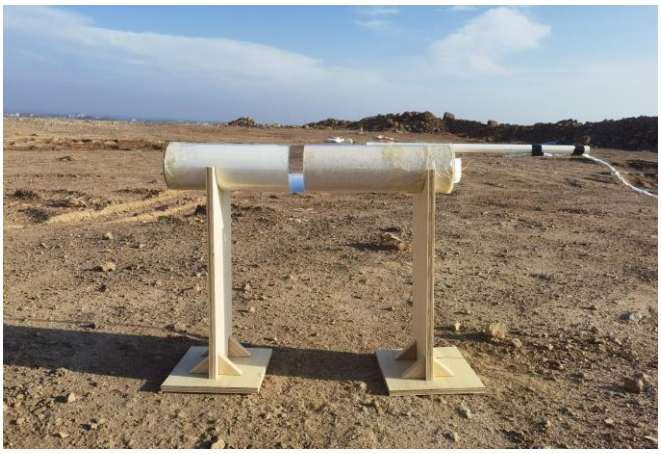

Fig. 9 Real picture of shock wave device

2.4.2. Experimental principle

During the experiment, the explosive is detonated and quickly reaches a stable detonation. The shock wave reaches the PMMA, and the state A of the PMMA is determined by its positive Hugoniot line and the wave line with a slope of $\rho_g D_g$ (Fig. 10). After the attenuation of the PMMA, the shock wave reaches the PMMA coral sand interface, transmits the shock wave, and reflects the sparse wave. The state B of the coral sand is determined by the intersection point along the isentropic line of the plexiglass and the zero initial wave line with the slope of the coral sand $\rho_c D_c$. In this way, an impact adiabatic state of coral sand under a certain impact pressure can be obtained. By changing the thickness of PMMA to adjust the impact pressure of different strengths, the Hugoniot line of coral sand can be fitted by several experiments

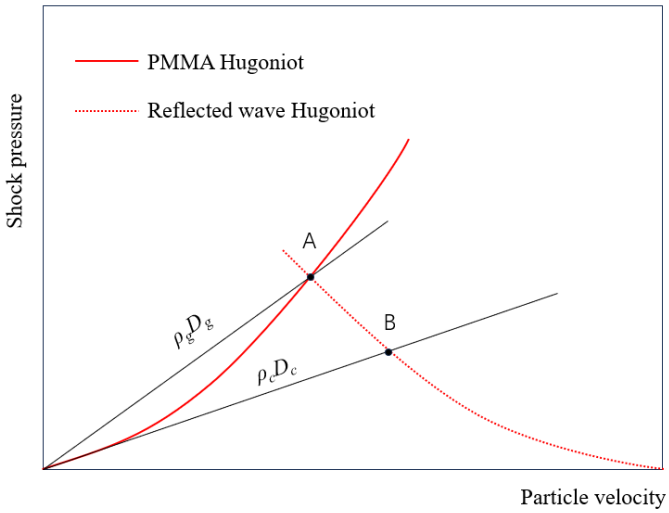

Fig. 10 Shock wave principle

3. Results and Discussion

After obtaining the voltage signal, the shock wave time history curve can be obtained through the transformation of formula (2), as shown in Fig. 11, where the red, green, and blue lines are respectively the shock wave time history curves in explosives, PMMA and coral sand.

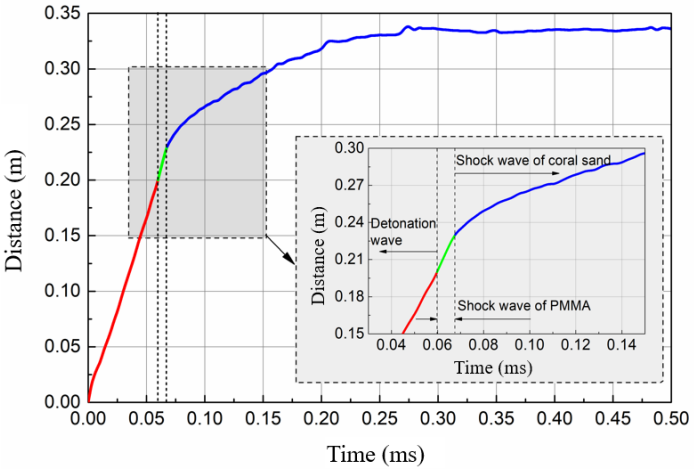

Fig. 11 Shock wave time history curve

The results of the 8 tests are shown in Fig. 12. By taking a small section before and after the interface between PMMA and coral sand, the shock wave velocity U_{s1} in PMMA and the shock wave velocity U_{s2} in coral sand can be obtained by derivation, and the results are shown in Table 3.

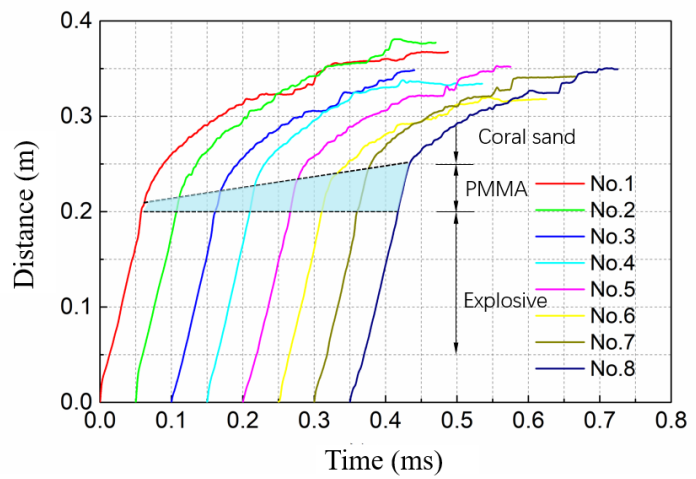

Fig. 12 shock wave time history curve for 8 tests

Table 3. Shock wave-related data table for 8 tests

Number	h_{PMMA}/(mm)	ρ_c/(g·cm^{-3})	U_{s1}/(km·s^{-1})	U_{s2}/(km·s^{-1})
1	15	1.406	3.7154	1.7019
2	20	1.441	3.5649	1.5694
3	25	1.435	3.4231	1.4995
4	30	1.402	3.3440	1.4807
5	35	1.337	3.1676	1.2618
6	40	1.374	3.0545	1.0662
7	45	1.392	2.8251	0.9490
8	50	1.398	2.6879	0.7124

After obtaining the shock wave velocity in PMMA and coral sand, the impedance matching method was used to calculate the impact state of coral sand under 8 different impact pressures. The results of the wavefront and waveback state of the PMMA-coral sand interface can be analyzed as shown in Table 4.

Table 4. PMMA - coral sand wave before and after data table for 8 tests

Number	Incident Wave		Transmitted Wave	
	P_A/(*Gpa*)	U_{pA}/(km·s^{-1})	P_B/(*Gpa*)	U_{pB}/(km·s^{-1})
1	0.3092	0.097	0.1540	0.144
2	0.6199	0.185	0.3470	0.262
3	1.1955	0.330	0.6804	0.459
4	1.3416	0.364	0.9165	0.466
5	1.5142	0.403	0.9339	0.540
6	2.0425	0.515	1.3250	0.670
7	2.2938	0.565	1.5234	0.725
8	2.7736	0.656	1.8731	0.832

The state data extracted from coral sand is the impact adiabatic (Fig. 13). Compared with quartz sand, the overall trend is lower, which is mainly due to the higher porosity and lower density of coral sand.

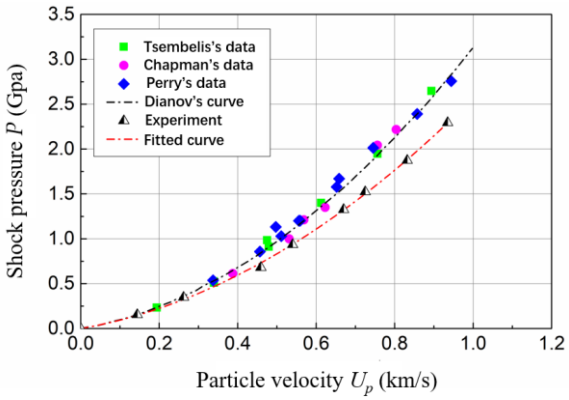

Fig. 13 Hugoniot line of coral sand and silica sand [29,35]

4. Discrete element simulation of shock wave propagation in coral sand

4.1. Establishment of numerical model

Based on the discrete element software PFC3D, a cylindrical rigid container was established, and coral sand particles of specific particle size groups were generated inside, as shown in Figure 14. Meanwhile, multiple measurement balls were continuously set along the shock wave path to simulate the function of continuous resistance probes. Two rigid plates were used to compact the coral sand particles at high speed, i.e., an initial velocity was applied to the push plate at the left end, while the sealing at the right end was removed. The incident shock wave was adjusted by regulating the initial velocity and loading time of the loading plate. The discrete element parameters are shown in Table 5.

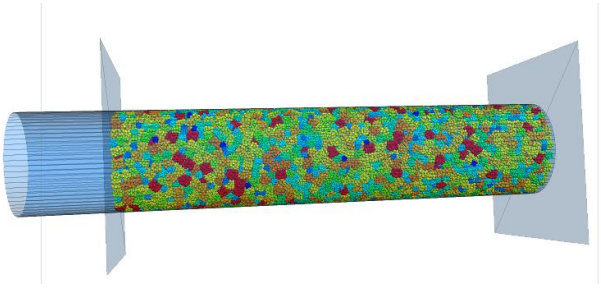

Graph 14 A Discrete Element Model for Shock Wave Propagation in Coralline Sand

Table 5 Basic parameters of the discrete element model

Tab. 5 Basic parameters of the DEM model

Function category	parameter	Symbol	Numerical value
parallel cementation model	effective modulus of elasticity [Pa]	$\bar{E}$	1.4×10^{9}
	Stiffness Ratio [-]	$\bar{k}_n / \bar{k}_s$	1
	tensile strength[Pa]	$\bar{\sigma}_c$	4×10^{7}

	cementation cohesion[Pa]	$\bar{c}$	4×10^7
	Cohesive internal friction angle[°]	$\bar{\phi}$	45
linear contact model	Effective Elastic Modulus[Pa]	E	1.4×10^9
	Stiffness Ratio [-]	k_n/k_s	1
	Friction Coefficient[-]	μ	0.5
Physical parameters of the model	Density[kg/m³]	ρ	2790
	Damping coefficient [-]	β	0.7
	Damping coefficient[m/s²]	g	-9.8

. 369

4.2 Particle diameter influence

By filling six different particle sizes of coral sand (with the same particle size range as shown in Fig. 2) separately and extracting the pressure data of each particle size, the shock wave pressure-distance curves of each particle size group can be obtained (Fig. 15(a)). The attenuation rate curves are plotted as shown in Fig. 15(b). As can be seen from the figures, the shock wave attenuation rates of coral sand with different particle sizes at different locations show certain differences. This is because for coral sand samples with different particle sizes, their shock wave attenuation characteristics are affected by both particle properties (elasticity, damage) and particle gap. Even in the same container under natural accumulation, sand with different particle sizes can hardly maintain the same particle gap. Therefore, this paper uses discrete element method to consider the influence of these two factors separately.

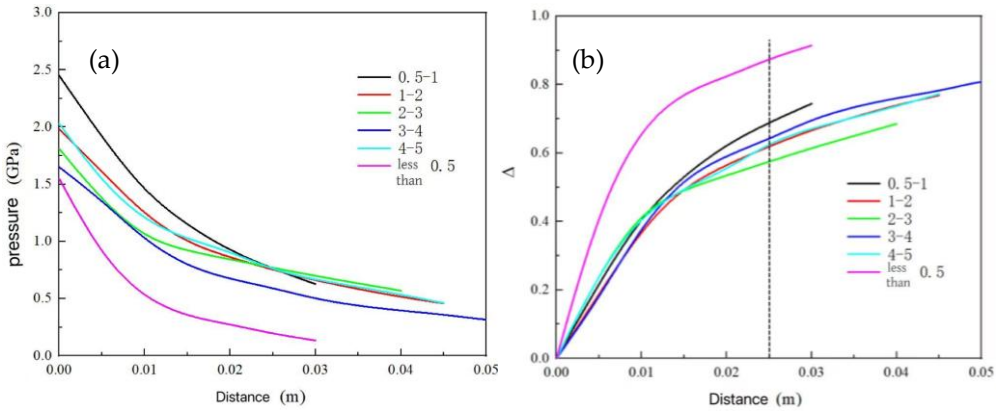

Graph 15 Particle Size Experimental Numerical Simulation:

(a) Pressure curves of different particle sizes; (b) Attenuation Rate Curves of Different Particle Sizes

Fig.15 Numerical simulation of particle size experiment: (a) pressure curves for each particle size; (b) decay rate curves for each particle size

4.2.1 Particle intrinsic property influence

This paper selects particles with a diameter of 2-3 mm and assigns them the properties of the other five particle sizes while keeping other conditions constant. Under these conditions, the particles in the container will maintain the same particle contacts and particle gaps, allowing us to investigate the impact of different particle properties on shock wave attenuation. After the program outputs the pressure-time curve, it is processed into a pressure-distance curve as shown in Figure 16(a), and the attenuation rate curve as shown in Figure 16(b). From the figures, it can be seen that, excluding the influence of particle contacts and particle gaps, larger particles exhibit faster attenuation effects.

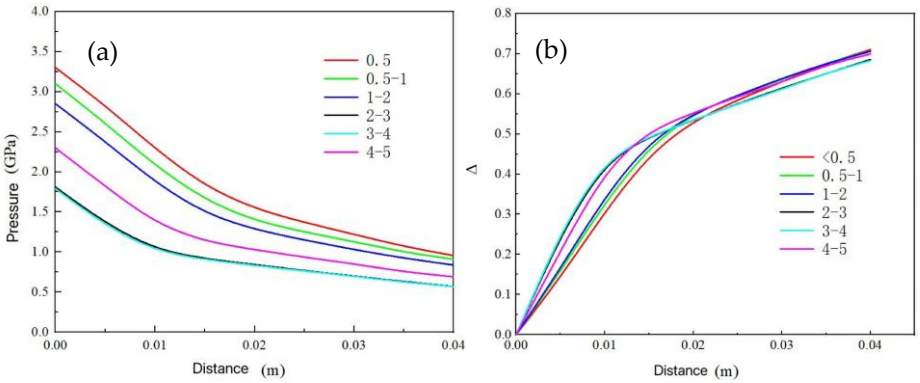

Graph 16 Numerical simulation with particle properties as variables:

(a) Pressure Curve; (b) Decay Rate Curve

Fig. 16 Numerical simulation with particle properties as variables: (a) pressure curves; (b) decay rate curves

4.2.2 Particle Gap Effect

Using particles with a size range of 2-3 mm, set the porosity at 0.3, 0.4, 0.5, and 0.6. The pressure-distance curves are shown in Figure 17(a), and the attenuation rates are shown in Figure 17(b). As can be seen from the figures: The attenuation rate of coral sand with large porosity is slightly higher than that with small porosity in the near field, but significantly lower in the far field. This is because the coral sand particles with larger porosity have a smaller coordination number and larger movement space. Under the action of shock waves, high-speed particles intensify collisions and friction, resulting in relatively greater energy dissipation. In the later stage, as the peak value of the shock wave decreases significantly, the particle velocity also decreases substantially, and the friction effect becomes less noticeable. At this point, the role of coral sand particles with smaller porosity in transmitting and reflecting interfaces becomes prominent, causing further attenuation of the shock wave.

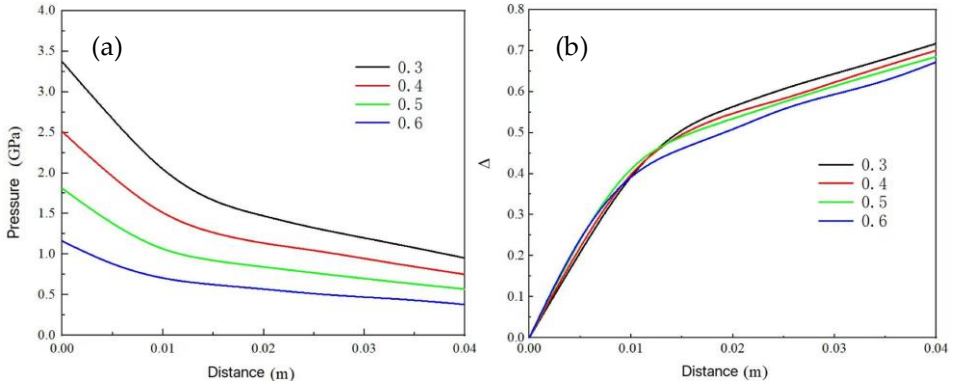

Graph 17 Numerical Simulation with Particle Gap as Variable:

(a) Pressure Curve; (b) Decay Rate Curve

Fig. 17 Numerical simulation of particle gap as variable: (a) pressure curves; (b) decay rate curves

4.3 Gradation Effect

When coral sand of different particle sizes is added to the container according to natural grading and uniform grading, the small-particle-size coral sand particles will be interspersed between the large-particle-size coral sand particles, which greatly improves the coordination number of coral sand particles. After loading, the pressure-distance curve and attenuation rate are shown in Figure 18. The shock wave attenuation effect of uniformly graded coral sand in the near field is higher than that of naturally graded coral sand, while in the far field the two are relatively close.

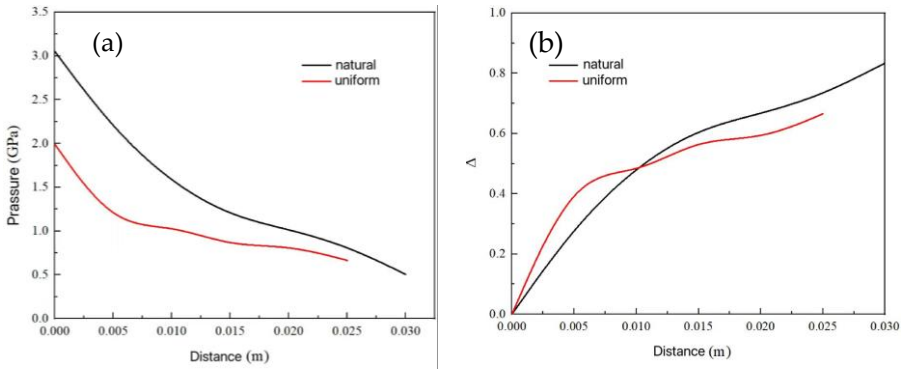

Graph 18 Gradation Test Numerical Simulation: (a) Pressure Curve ; (b) Decay Rate Curve

Fig. 18 Numerical simulation of grading experiment: (a) pressure curves; (b) decay rate curves

Observe the evolution process of its parallel bonds (Figure 19(a)). In the figure, green represents unbroken bonds, gray indicates shear failure of bonds, and red signifies tensile failure of bonds. This shows that most coral sand undergoes shear failure under shock wave action. Since shear force comes from friction, it indicates that inter-particle friction plays an important role in shock wave attenuation. The propagation path of the shock wave can be clearly seen from the bond breakage patterns. A slice observation of its force chains is shown in Figure 19(b). At 5 us, the force chains in the shock wave affected area are very dense, indicating high particle packing density, which is a manifestation of impact compaction. The thickness of the force chains also shows that this area is under high stress. Looking at 10 us and 15 us, it can be seen that the shock wave front gradually becomes sparser, reflecting the attenuation effect of the shock wave.

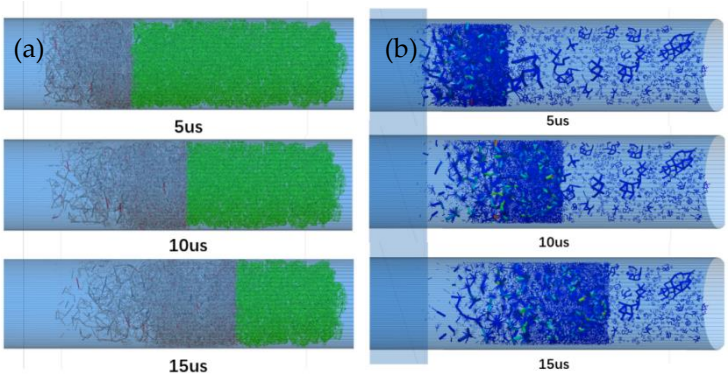

Graph 19 Gradation Experiment Numerical Simulation Analysis:

(a) Parallel Key Evolution ; (b) Force Chain Evolution

Fig. 19 Numerical simulation analysis of grading experiment: (a) parallel bond evolution ;(b) force chain evolution

5. Conclusions

In this paper, the state equation of coral sand shock was obtained by using the pressure conductance continuous resistance wire probe, chemical explosion loading technology and continuous resistance measurement technology, and autodyn was used to simulate the attenuation effect of the material on shock wave under certain conditions. The main conclusions are as follows:

1) For the study of high-pressure physics of large heterogeneous materials such as granular materials, chemical explosion loading is a common loading method in field testing, and the voltage conductance resistance wire probe brings great convenience to the field measurement of a shock wave，

2) The detonation wave and shock wave data of explosives, standard materials (PMMA), and coral sand were measured successfully by a shock wave test device based on a continuous resistance probe. The shock was adiabatic of coral sand and was measured by the shock wave impedance matching principle。

3) Excluding the effects of particle contact and particle gap, larger coral sand particles exhibit faster shock wave attenuation; coral sand with higher porosity shows rapid shock wave attenuation at the proximal end, while coral sand with lower porosity demonstrates more significant shock wave attenuation at the distal end. The grading simulation reflects that most coral sand undergoes shear failure under shock wave action, with friction playing a crucial role. The parallel bond evolution diagram clearly displays the shock wave propagation process, and the force chain diagram effectively demonstrates the phenomenon of shock wave attenuation.

Funding: This work was supported by the National Natural Science Foundation of China (Grant No. 12202217), Zhejiang Provincial Natural Science Foundation of China (Grant No. LMS25A020006), the Opening Project of State Key Laboratory of Explosion Science and Technology (Beijing Institute of Technology) (KFJJ21-19M) and the Natural Science Foundation of Ningbo,China (Grant No. 2021J122).

References

1. Liu C.Q.; Yang Z.Q.; Wang R. The present condition and development in studies of mechanical properties of calcareous soils. Rock Soil Mech. 1995, 16(4), 74-83.
2. Liu C.Q.; Wang R. Preliminary research on physical and mechanical properties of calcareous sand. Rock Soil Mech. 1998, 19(3), 32-37.
3. Tang G.Y.; Zheng J.G. Engineering properties of reef calcareous rock in Southeast Asia. Geotechnical Investigation & Surveying. 2015, 43(06), 6-10. (In Chinese)
4. Lv, Y.R.; Wang, C.; Hang, H.X.; Zuo, D.J. Study on particle structure and crushing behaviors of coral sand. Rock Soil Mech. 2021, 42(02), 352-360.
5. Ma, D.H.; Han, X.; Guan, Y.F.; Tang, Z. Pore structure and seepage characteristics analysis of coral sand particles. Rock Soil Mech. 2022, 43(S2), 223-230.
6. Zang X.Y.; Cai, Y.Y.; Wang Z.B.; Jiang, Y.Q. Fractal breakage and particle shape analysis for coral sand under high-pressure and one-dimensional creep conditions. Rock Soil Mech. 2018, 39(05), 1573-1580.
7. Cui, X.; Hu, M.J.; Zhu, C.Q.; Wang, R.; Wang Z.X.; Wang, T.M. Study on the microscopic characteristics of three-dimensional poresin coral sand. Rock Soil Mech. 2020, 41(11), 3632-3640+3686.
8. Liu, Z.W; Li, C.; Hu, X. Experimental study on engineering properties of coral reef calcareous rock. Geotechnical Investigation & Surveying. 2012, 40(09), 17-21. (In Chinese)
9. Tang, G.Y.; Zheng, J.G. Engineering properties of reef calcareous rock in Southeast Asia. Geotechnical Investigation & Surveying. 2015, 43(06), 6-10. (In Chinese)
10. Wu, X.H.; Cai, Y.Q.; Xu, S.F.; Zhuang, Y.C.; Wang, Q.X.; Wang, Z. Effects of size and shape on the crushing strength of coral sand particles under diametral compression test. Bull Eng Geol Environ. 2021, 80, 1829–1839.
11. Wang, C.Y.; Ding, X.M.; Xiao, Y.; Peng, Y.; Liu, H.L. Effects of relative densities on particle breaking behaviour of non-uniform grading coral sand. Powder Technol. 2021, 382, 524-531.
12. Wang, T.Y.; Ma, L.J.; Wang, M.Y.; Li, Z.; Zhang, X.; Geng, H.S.; Effects of particle shape on dynamic mechanical behaviours of coral sand under one-dimensional compression. Eng Geol. 2022, 304, 106624.
13. Peng, Y.; Ding, X.M.; Xiao, Y.; Deng, X.; Deng, W.T. Detailed amount of particle breakage in nonuniformly graded sands under one-dimensional compression. Can Geotech J. 2020, 57(8), 1239-1246.
14. Wang, J.B.; Fan, P.X.; Wang, M.Y.; Dong, L.; Ma, L.J.; Gao, L. Experimental study of one-dimensional compression creep in crushed dry coral sand. Can Geotech J. 2020, 57(12), 1854-1869.
15. Suescun-Florez, E.; Iskander, M.; Bless, S. Evolution of particle damage of sand during axial compression via arrested tests. Acta Geotech. 2020, 15, 95-112.

16. Wang, C.; Ding, X.; Yin, Z.Y.; Peng, Y.; Chen, Z.X. Mechanical characteristics and particle breakage of coral sand under one-dimensional repeated loading. Acta Geotech. 2022, 17, 3117-3130.
17. Dehnavi, Y.; Shahnazari, H.; Salehzadeh, H.; Rezvani, R.; Compressibility and undrained behavior of hormuz calcareous sand. Electron. J. Geotech. Eng. 2010, 15(1), 1684-1702.
18. Wu, Y.; Cui, J.; Li, N, Wang, X.; Wu, Y.H.; Guo, S.Y. Experimental study on the mechanical behavior and particle breakage characteristics of hydraulic filled coral sand on a coral reef island in the South China Sea. Rock Soil Mech. 2020, 41(10), 3181-3191.
19. Li, J.G.; Wang, R.; Yu, H.Z.; He, Y.; Xu, C.X. Experimental research on effect of initial principal stress orientation on dynamic properties of calcareous sand. Rock Soil Mech. 2005, 26(5), 723-727
20. Liang, K.; He, Y.; Cheng, G.X.; Experimental study of dynamic shear modulus and damping ratio characteristics of coral sand from Nansha Islands. Rock Soil Mech. 2020, 41(01), 23-31+38.
21. Liang, K.; Cheng, G.X.; Liu, K.; Wang, Y.Z.; Degradation properties and prediction model of maximum shear modulus of saturated coral sand under cyclic triaxial loading. Rock Soil Mech. 2020, 41(02), 601-611.
22. Zhou, G.; Li, Y.L.; Li, J; Wu, Z.T.; Wu, K.; Jing, J.Y.; Tan, S.S.; Qian, B.W. ; Zhu, Y.R.; Zhang, X.G. Dynamic behavior of clay with different water content under planar shock conditions. Int. J. Impact. Eng. 2019, 129, 57-65.
23. Arlery, M.; Gardou, M.; Fleureau, J.M.; Mariotti, C. Dynamic behaviour of dry and water-saturated sand under planar shock conditions. Int. J. Impact. Eng. 2010, 37, 1-10.
24. LaJeunesse, J.W.; Hankin M.; Kennedy, G.B.; Spaulding, D.K.; Schumaker, M.G.; Neel, C.H.; Borg, J.P.; Stewart, S.T.; Thadhani, N.N. Dynamic response of dry and water-saturated sand systems. J. Appl. Phys. 2017, 122 (1), 015901.
25. Ding, Y.Q.; Tang, W.H.; Zhang, R.Q.; Rang, X.W.; Zhang, J.M. Equation of State for Unsaturated Clay by Plate Impact Experiments. Chin. J. High Pressure Phys. 2014, 28(06), 648-654. (In Chinese)
26. Tobias, H.; Frank, B.; Stefan H. Hugoniot data of Seeberger sandstone up to 7 GPa. Int. J. Impact. Eng. 2017, 99, 122-130.
27. Jeff W, L.; John P, B.; Sarah T, S.; Naresh N, T. Investigating the shock response of dry and water-saturated sand: Flyer-plate experiments and mesoscale simulations. AIP Conf. Proc. 2018, 1979 (1), 110007.
28. Liu, C.; Wu, Y.; Zhang, X.F.; Deng, J.J.; Xu, C.Y.; Xiong, W.; Tan, M.T. Propagation of shock waves in dry and wet sandstone: Experimental observations theoretical analysis and meso-scale modeling. Def Technol. 2018, 14, 513-521.
29. Chapman, D.J.; Tsembelis, K.; Proud, W.G. The Behaviour of Dry Sand under Shock-Loading. AIP Conf. Proc. 2006, 845(1), 1445–1448.
30. (31)Wang, X.; Cui, J.; Wu, Y.; Zhu, C.Q.; Wang, X.Z. Mechanical properties of calcareous silts in a hydraulic fill island-reef. Mar. Georesour. Geotechnol. 2021, 39(1), 1-14.
31. LI, K.B.; DONG, X.L.; WANG, Y.G.; CHEN, X.; LI, X.J.; Continuous resistance test method in determining the attitude of flyer plate driven by sliding detonation. Explos. Shock Waves. 2021, 41(5), 105 -114. (In Chinese)
32. LI, K.B.; LI, X.J.; WANG, X.H.; YAN, H.H. Study of continuous velocity probe method for near-field underwater explosion measurement of spherical charge. Acta Armamentarii. 2019, 40(1), 1 -7. (In Chinese)
33. LI, K.B.; LI, X.J.; YAN, H.H. A continuous resistance wire probe method for determining the critical diameter and thickness of commercial explosives. Chin. J. Energ. Mater. 2018, 26(7), 620 -625. (In Chinese)
34. LI, K.B.; LI, X.J.; YAN, H.H. The mechanism analysis of noise wave in detonation velocity continuous measurement. Engineering Blasting, 2017, 23(5), 85 -90. (In Chinese)
35. Perry, J.I.; Braithwaite, C.H.; Taylor, N.E. Behaviour of moist and saturated sand during shock and release. Appl Phys Lett. 2015, 107(17), 174102.